Bichromatic Wave Selection for Validation of the Difference-Frequency Transfer Function for the OC6 Validation Campaign

Preprint

Nathan Tom[1], Amy Robertson[1], Jason Jonkman[1], Fabian Wendt[1], and Manuela Böhm[2]

1 National Renewable Energy Laboratory
2 Institute of Structural Analysis, Leibniz Universitat Hannover

Presented at the International Offshore Wind Technical Conference (IOWTC)
St. Julian's, Malta
November 3–9, 2019

NREL is a national laboratory of the U.S. Department of Energy
Office of Energy Efficiency & Renewable Energy
Operated by the Alliance for Sustainable Energy, LLC

This report is available at no cost from the National Renewable Energy Laboratory (NREL) at www.nrel.gov/publications.

Contract No. DE-AC36-08GO28308

Conference Paper
NREL/CP-5000-73929
December 2019

Bichromatic Wave Selection for Validation of the Difference-Frequency Transfer Function for the OC6 Validation Campaign

Preprint

Nathan Tom[1], Amy Robertson[1], Jason Jonkman[1], Fabian Wendt[1], and Manuela Böhm[2]

1 National Renewable Energy Laboratory
2 Institute of Structural Analysis, Leibniz Universitat Hannover

Suggested Citation
Tom, Nathan, Amy Robertson, Jason Jonkman, Fabian Wendt, and Manuela Böhm. 2019. *Bichromatic Wave Selection for Validation of the Difference-Frequency Transfer Function for the OC6 Validation Campaign: Preprint*. Golden, CO: National Renewable Energy Laboratory. NREL/CP-5000-73929. https://www.nrel.gov/docs/fy20osti/73929.pdf

NREL is a national laboratory of the U.S. Department of Energy
Office of Energy Efficiency & Renewable Energy
Operated by the Alliance for Sustainable Energy, LLC

This report is available at no cost from the National Renewable Energy Laboratory (NREL) at www.nrel.gov/publications.

Contract No. DE-AC36-08GO28308

Conference Paper
NREL/CP-5000-73929
December 2019

National Renewable Energy Laboratory
15013 Denver West Parkway
Golden, CO 80401
303-275-3000 • www.nrel.gov

NOTICE

This work was authored in part by the National Renewable Energy Laboratory, operated by Alliance for Sustainable Energy, LLC, for the U.S. Department of Energy (DOE) under Contract No. DE-AC36-08GO28308. Funding was provided by the U.S. Department of Energy Office of Energy Efficiency and Renewable Energy Wind and Water Technologies Office. The views expressed herein do not necessarily represent the views of the DOE or the U.S. Government. The U.S. Government retains and the publisher, by accepting the article for publication, acknowledges that the U.S. Government retains a nonexclusive, paid-up, irrevocable, worldwide license to publish or reproduce the published form of this work, or allow others to do so, for U.S. Government purposes.

Cover Photos by Dennis Schroeder: (clockwise, left to right) NREL 51934, NREL 45897, NREL 42160, NREL 45891, NREL 48097, NREL 46526.

BICHROMATIC WAVE SELECTION FOR VALIDATION OF THE DIFFERENCE-FREQUENCY TRANSFER FUNCTION FOR THE OC6 VALIDATION CAMPAIGN

Nathan Tom[1], Amy Robertson, Jason Jonkman, Fabian Wendt
National Renewable Energy Laboratory
Golden, Colorado (USA)

Manuela Böhm
Institute of Structural Analysis
Leibniz Universität Hannover
Hannover, Germany

ABSTRACT

The focus of the Offshore Code Comparison Collaboration, Continuation, with Correlation and unCertainity (OC6) project, which operates under the International Energy Agency Wind Task 30, is to refine the accuracy of engineering tools used to design offshore wind turbines. In support of this work, a new validation campaign is being developed that seeks to better understand the nonlinear wave loading that excites floating wind systems at their low-frequency, rigid-body modes in surge and pitch. The validation data will be employed in a three-way validation between simplified engineering tools and higher-fidelity tools, such as computational fluid dynamics (CFD). Irregular wave spectrums, which are traditionally used to examine the nonlinear wave interaction with offshore structures, are too computationally expensive to be simulated in CFD tools, and so we will employ bichromatic wave cases instead. This paper reviews the process used to choose the bichromatic wave pairs to be applied in the campaign to validate the second-order difference-frequency quadratic and potential loads at the surge and pitch natural frequencies of a floating semisubmersible.

Keywords: Offshore wind, bichromatic waves, nonlinear hydrodynamics, second-order difference-frequency

1 INTRODUCTION

Within Phase II of the Offshore Code Comparison Collaboration, Continued, with Correlation (OC5) project, participants validated coupled engineering-level physics-based models of a floating semisubmersible tested in the ocean basin at the Maritime Research Institute Netherlands (in May 2013) by the DeepCwind consortium [1]. Although state-of-the-art tools captured many of the dynamics and loads of the complex floating wind turbine, there were persistent differences between the simulated loads/motion of the system and measurements. The largest differences were associated with the low-frequency response at the semisubmersible's pitch and surge natural frequencies. Semisubmersible designs typically place their rigid-body natural frequencies below the primary frequency region of the waves to avoid large excitations. However, a nonlinear phenomenon created by the interaction between the frequency components in an irregular wave spectrum can create excitation at frequencies at the sum and difference of the individual wave component frequencies. The nonlinear excitation loads are small, but because of their resonant nature, can result in large motions at the rigid-body natural frequencies. Both an underprediction of this nonlinear loading, combined with an overprediction (or misrepresentation) of the damping in the system, are assumed to be the cause for the underprediction of the low-frequency loads/response by simulation tools in the OC5 project.

Within a new extension of the OC5 project, the Offshore Code Comparison Collaboration, Continued, with Correlation, and unCertainty (OC6) project, participants are seeking to try to better understand the reason for this underprediction through additional testing and comparison to higher-fidelity modeling tools, such as computational fluid dynamics (CFD). One drawback of the higher-fidelity tools is that their large computational time makes it difficult to study long simulations, which are needed to examine the low-frequency response characteristics from irregular waves. Therefore, an alternative approach was needed to study the nonlinear wave phenomenon with CFD tools. The approach applied in the OC6 project is to excite the semisubmersible using a bichromatic wave spectrum instead. A simple bichromatic wave spectrum can be generated by adding together two regular waves at different frequencies. By choosing frequencies whose difference aligns with the pitch and surge natural frequencies, the nonlinear (difference-frequency) wave excitation can be studied with decreased computational cost versus an irregular wave case.

[1] Contact author: Nathan.Tom@nrel.gov

Other researchers have also examined the nonlinear response of floating systems using bichromatic waves. Simos et al. [2] studied the slow-drift response behavior of a semisubmersible offshore wind system through excitation with bichromatic waves, and saw that they were able to match well with quadratic transfer function (QTF) estimations. Shao and Faltinsen [3] used a similar approach to examine the springing phenomenon in ships resulting from sum-frequency excitation with bichromatic waves. You and Faltinsen [4] studied the slowly varying surge motion of a liquefied natural gas carrier model using bichromatic waves in a head sea, and compared the numerical results with experimental data from Marintek. Ohyama and Hsu [5] examined the motion of a rectangular floating body in response to nonlinear bichromatic waves to examine the validity range of a second-order approximation.

The focus of this paper is to develop bichromatic wave cases for use in a new validation campaign to be performed within OC6. The validation campaign will look at the loads on individual components of the OC5-DeepCwind semisubmersible, and with the components interconnected, to understand how the nonlinear wave loading changes when members are in close proximity to each other; and, whether engineering-level tools and CFD can predict the correct nonlinear wave loading. The load cases developed here will focus on examining both the pitch and surge natural frequencies, and are chosen based on identifying frequencies where the QTFs from WAMIT are large and have high wave energy.

The remainder of the paper focuses first on the modeling approach used to represent the nonlinear wave phenomenon of interest in the engineering-level tools. The development of the QTF in WAMIT is then discussed, as well as its sensitivity to different parameter settings. From the QTF, load cases are defined based on the regions in the QTF with the largest magnitude. Finally, the influence of the WAMIT settings on the simulated response of the floating semisubmersible in the engineering-level tools are examined, as well as the differences in the load levels at the pitch and surge natural frequencies when considering an irregular wave spectrum versus a bichromatic wave, which will capture just a portion of the response magnitude.

2 MODELING APPROACH

2.1 Geometry Description

The validation campaign to be performed within OC6 will examine the loads on individual components of the OC5-DeepCWind semisubmersible [1] under wave loading in a fixed condition while being forced to oscillate in multiple degrees of freedom (DOF). The individual components include an isolated cylinder and an isolated cylinder with a heave plate/base column (labeled “Assembly 1”). The primary dimensions of the isolated components can be found in TABLE 1, with a visualization of the low-order geometric data file (GDF) of WAMIT for each component shown in FIGURE 1 and FIGURE 2.

TABLE 1: FULL-SCALE COMPONENT DIMENSIONS

Cylinder Dimensions		
Draft	14	m
Radius	6	m
Assembly 1 Dimensions		
Cylinder Dimensions		
Draft	14	m
Radius	6	m
Heave Plate Dimensions		
Height	6	m
Radius	12	m

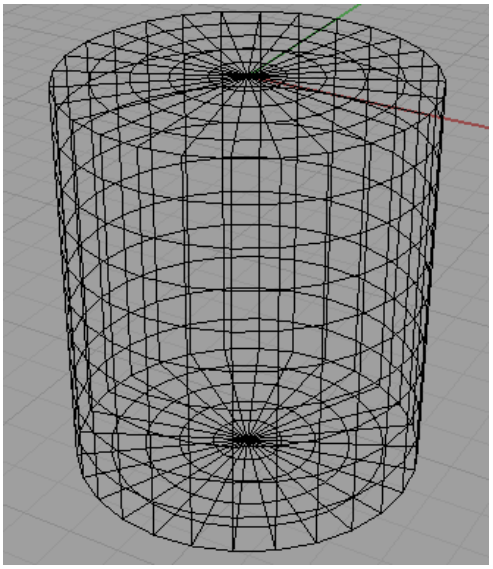

FIGURE 1: ISOMETRIC VIEW OF THE LOW-ORDER GDF FOR THE CYLINDER WITH 290 PANELS WITH AN AVERAGE PANEL SIZE OF 1 M.

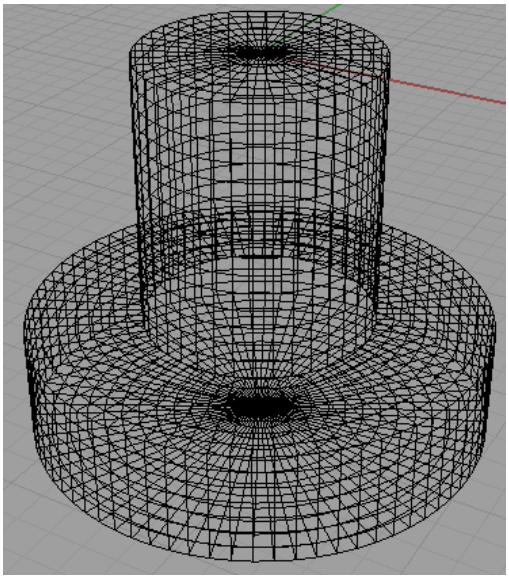

FIGURE 2: ISOMETRIC VIEW OF THE LOW-ORDER GDF FOR ASSEMBLY 1 WITH 733 PANELS (AVERAGE PANEL SIZE IS 1 M).

The authors will study these components in isolation, and then perform tests with three of these column/heave plate combinations combined (labeled, "Configuration 1"), resembling the full OC5-semisubmersible (see FIGURE 3); but, without the smaller central main column and cross members (pontoons/braces). Through building up the system's geometric complexity, we can better understand if engineering tools can accurately represent the hydrodynamic loading when members are in close proximity to each other. The center locations of the semisubmersible columns at full scale are given in TABLE 2.

TABLE 2: CONFIGURATION 1 COLUMN LOCATIONS

Column Number	X [m]	Y [m]
1	-22.730	0
2	11.365	-19.685
3	11.365	19.685

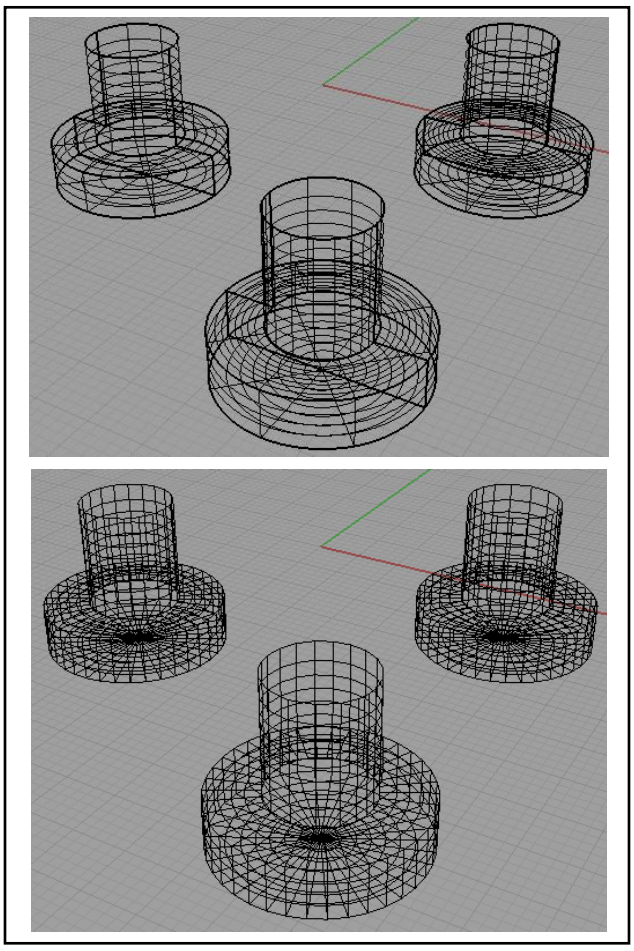

FIGURE 3: (TOP) ISOMETRIC VIEW OF THE HIGHER-ORDER GDF FOR CONFIGRATION 1 AND (BOTTOM) ISOMETRIC VIEW OF THE LOW-ORDER GDF FOR CONFIGURATION 1, WITH 1095 PANELS (AVERAGE PANEL SIZE IS 2 M).

2.2 OpenFAST Model Description

The modeling tools that are the focus of the validation work within OC5 and OC6 are coupled aero-hydro-servo-elastic modeling tools; meaning that they simultaneously consider the wind loads, wave loads, structural dynamics, and controller interactions in a coupled manner. Although these engineering-level tools capture many of the important physics, they do not fully represent the nonlinear behavior of these components, but rather use simplified models that are computationally efficient.

One such simulation tool, OpenFAST [6], is used in this study. The hydrodynamic loading module in OpenFAST, HydroDyn, uses a time-domain approach that includes a hybrid combination of a potential-flow model (for large-volume bodies), with additional viscous drag computed via the drag term from Morison's equation:

$$F_D = \frac{1}{2} C_D \cdot \rho \cdot A \cdot (u - \dot{q}) \cdot |u - \dot{q}|$$

Where C_D is the drag coefficient, ρ the water density, A the cross section of the structural member, u the flow velocity, and $\dot{q}$ the velocity of the structure [10].

The potential-flow model is based on the time-domain transform of the frequency-dependent wave diffraction excitation and radiation added mass and wave damping matrices from WAMIT [7], as well as the second-order sum- and difference-frequency wave-excitation loads from QTFs also derived from WAMIT. The linear potential-flow model assumes that the fluid is inviscid, incompressible, and irrotational while the floating body experiences small amplitude motion under low steepness waves. These assumptions require the addition of tuning parameters, such as Morison's equation (in a hybrid manor), to account for nonlinear viscous effects that can be captured directly from CFD.

An OpenFAST model is used in this study to examine the sensitivity of the WAMIT modeling approach on the low-frequency response of the system. The OpenFAST model focuses solely on Configuration 1 (three upper and three base columns) with potential-flow and Morison terms considered. The wave kinematics used in the viscous-drag calculation include wave stretching and second-order difference-frequency terms [8]. The drag forces were calibrated with free-decay tests from a set of experiments to be examined in OC6 Phase I. The axial drag coefficient (Cd) was calibrated using heave- and pitch-decay tests, whereas the transverse Cd for the upper and base columns was calibrated using the surge- and pitch-decay tests. An axial Cd of 8.2 (applied only to the bottom surface of the base column), and a transverse Cd of 1.6 for the upper columns and 0.4 for the base columns, led to the best results and are used in this study, unless stated otherwise.

2.3 WAMIT Model Description

We modeled the isolated components in WAMIT using analytic representations of each geometry with two planes of symmetry. The advantage of using the analytic representation of the geometry is the ability to use the higher-order method in WAMIT, which is generally more computationally efficient and accurate. The higher-order method tends to converge faster than the lower-order method as the number of panels are increased. The number of panels can be controlled by setting the PANEL_SIZE parameter in the WAMIT configuration file. The PANEL_SIZE parameter is used to create an automatic

subdivision of patches in the higher-order method. The patches will be subdivided into panels so that the maximum length of each panel is approximately equal to PANEL_SIZE in dimensional units. The patches refer to the distinct surfaces on the body geometry. For example, in FIGURE 1, the cylinder could have up to three patches that correspond to the top circular surface, tubular side surface, and bottom circular surface. The top circular patch, which represents the interior free surface, is not required to calculate the first- and second-order hydrodynamic calculations but is needed for WAMIT to remove irregular wave frequencies. When modeling Configuration 1, one geometric plane of symmetry was used, and a higher-order representation of the geometry came from a MultiSurf-generated surface file.

3 WAMIT QTF DEVELOPMENT

The QTFs are one of the two primary modeling components for representing the hydrodynamic loading of the semisubmersible at its pitch and surge natural frequencies; the other being the drag forces from the viscous-drag term of Morison's equation. Thus, one of the focuses of the OC6 campaign is validating the QTF values derived in WAMIT. Through the development of bichromatic wave cases, discrete points in the QTF can be validated from controlled wave tank experiments. WAMIT was used to identify the points in the QTF that have the largest contribution to the excitation of the system at its pitch and surge natural frequencies. In Sections 3.1 through3.2.2, the WAMIT models are examined to ensure that an accurate QTF is calculated.

3.1 WAMIT First Order Wave-Excitation Loads

We calculated the first-order wave-excitation loads using WAMIT Version 6.1 [7], with the forces outputted at the centerline of the structure at the still water line. The water depth was chosen to be infinite, which maintains the deep-water condition for all wave frequencies. The incident wave direction was set at 0 degrees and follows the WAMIT notation. The first-order wave-excitation forces and moments for the cylinder, Assembly 1 and Configuration 1, were all calculated by WAMIT for wave frequencies between 0.054 and 0.213 Hz at a spacing of 0.016 Hz. The OC6 validation campaign considers an irregular wave train that is described by a Joint North Sea Wave Project (JONSWAP) spectrum with a peak period of 12.1 s and significant wave height of 7.1 m. The 0.054 to 0.213 Hz range of frequencies was selected because wave amplitudes below and above these limits are less than 10% of the wave amplitude at the peak frequency, and the majority of energy in the wave spectrum is covered. To improve simulation accuracy in irregular sea states, a larger and denser wave frequency vector is needed, but for now the selected frequencies are enough for identifying biochromatic wave pairs to run as part of the OC6 validation campaign.

Although second-order difference-frequency wave forces and moments are of interest, hydrodynamic loads can be dominated by the first-order wave forces and moments. Therefore, understanding how the first-order wave forces and moments change between the cylinder, Assembly 1, and Configuration 1 is important. The first-order surge wave-excitation force and pitch wave-excitation moment have been plotted in FIGURE 4 and FIGURE 5, respectively. The first-order surge wave-excitation force is lowest for the isolated cylinder, which is expected given the cylinder has the smallest projected area along the surge axis (x-axis). Assembly 1 has a greater surge wave-excitation force than the cylinder given the addition of the heave plate with the largest difference occurring near 0.134 Hz; however, at the low and high ends of the frequency range, the surge wave-exciting forces begin to converge. In the low-frequency range, this is because the wave slope decreases, reducing the pressure difference on the front and back of the cylinder and Assembly 1. At the high-frequency end, the wave pressure will not penetrate as deep in the water column because of the exponential decay of wave pressure with depth and the geometry of importance for Assembly 1 becomes the upper column.

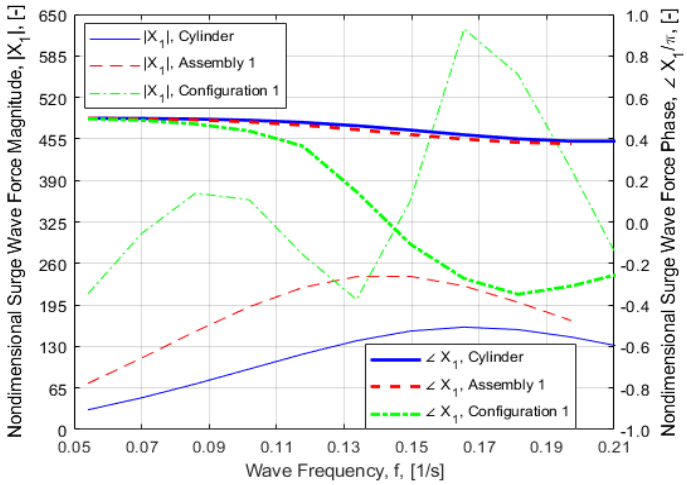

FIGURE 4: FIRST-ORDER SURGE WAVE-EXCITATION FORCE MAGNITUDE AND PHASE.

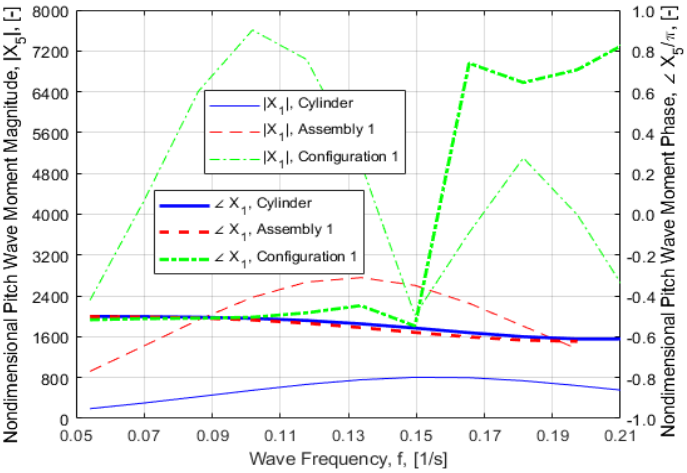

FIGURE 5: FIRST-ORDER PITCH WAVE-EXCITATION MOMENT MAGNITUDE AND PHASE.

In addition, the surge-wave excitation force phase for the cylinder and Assembly 1 is positive resulting in the surge-wave

excitation force peak to lead the crest of the incident wave. Over most of the frequency range, Configuration 1 has the largest surge wave-excitation force except near 0.134 Hz, wherein the magnitude drops below Assembly 1. This reduction is likely a result of interaction effects between the legs of the columns and the separation distance between the front and back columns. In addition, at frequencies above 0.134 Hz, the surge wave-excitation force phase becomes negative, which results in the maximum surge force occurring after the wave crest passes the origin. Similar trends can be observed for the first-order pitch wave-excitation moment except that the phase switches between approximately -π/2 to more than π/2 over a narrow frequency range of 0.015 Hz. This may be the result of interactions between columns when the wavelength is near or equal to the spacing between the front and back columns.

3.2 WAMIT Second-Order Wave-Excitation Loads

The second-order wave-excitation forces and moments were calculated using WAMIT Version 6.107S [7], which allows the structures to be either freely floating, constrained, or fixed. The capabilities of V6.107S include the sum- and difference-frequency components of the second-order forces and moments, otherwise known as the QTFs. In this work, we obtained only the difference-frequency QTFs from WAMIT. The verification of the difference-frequency QTF is a priority in the OC6 validation campaign as it is believed to be a main contributor to the underprediction of the semisubmersible response at the surge and pitch natural frequencies [1]. The total second-order forces and moments are the sum of two components. The first component is the quadratic forcing of the first-order potentials and the second component is the second-order potential. The second-order potential was calculated using the 'direct' method in WAMIT and is described in [7].

3.2.1 Component Difference-Frequency Quadratic Transfer Functions

The second-order surge wave-excitation force QTF magnitude for the cylinder, Assembly 1, and Configuration 1 are plotted in FIGURE 6, FIGURE 7, and FIGURE 8, respectively. In these plots, only the lower-right-half plane has been plotted as the second-order difference-frequency quantities satisfy the following symmetry relation:

$$X_{kij}^{(2)-} = X_{kji}^{(2)-*} \quad (1)$$

where the superscript (2) denotes second order, the superscript – denotes difference-frequency, the superscript * denotes the complex conjugate, k denotes the force or moment degree of freedom (1=surge, 2=sway, 3=heave, 4=roll, 5=pitch, 6=yaw), and the indices i,j denote the first and second wave frequencies. Therefore, values on the upper-left-half plane will mirror the lower-right-half plane when plotting the QTF magnitude. On these plots, the red dashed line identifies the bichromatic wave pairs that generate a difference frequency at the surge natural or pitch natural frequency. Furthermore, the QTFs are plotted in nondimensional form, as defined by WAMIT [7], which consists of dividing the dimensional values by the fluid density, gravitational acceleration, and the amplitudes of the first and second waves. Therefore, even though the nondimensional value of the QTF magnitude is large, it might not be located where there is substantial first order wave energy, and the second order forcing on the structure from the bichromatic wave pair can be diminished.

For the isolated cylinder, the surge wave-excitation QTF force magnitude has an ever increasing gradient when moving away from the lower left hand corner of FIGURE 6. In FIGURE 6, the surge wave-excitation QTF force magnitude has a larger gradient when moving along first wave frequency horizontal axis compared to the second wave frequency vertical axis. It will be of interest to select a bichromatic wave pair located along the steepest gradient to understand the frequency pair sensitivity of the QTF. The addition of the heave plate in Assembly 1 increases the peak surge force QTF to a value of over 8, with the peak remaining in the lower right hand corner of FIGURE 7.

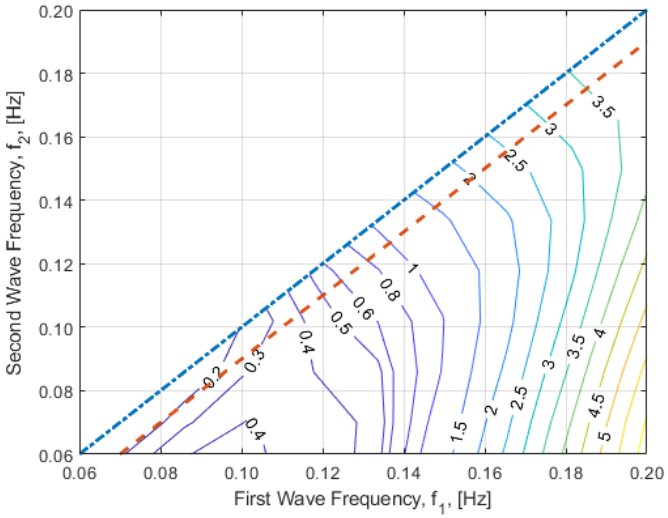

FIGURE 6: SECOND-ORDER SURGE WAVE-EXCITATION FORCE QTF MAGNITUDE FOR CYLINDER (AVERAGE PANEL SIZE OF 1 M).

The addition of two more columns in Configuration 1 leads to a ten-fold increase in the maximum surge force QTF, which is concentrated at the corner of the lower-half plane corresponding to the bichromatic wave pair with the smallest and largest wave frequencies used to calculate the QTF. Furthermore, Configuration 1 has a local peak located at a wave frequency pair of 0.197 and 0.181 Hz, which lies along the surge natural frequency line. The local peak along the surge natural frequency line is arguably more important for capturing and understanding the low-frequency response of the semisubmersible, which is the focus of the OC6 validation campaign. Therefore, the values of the surge wave-excitation force and pitch-excitation-moment QTFs along bichromatic wave pairs that produce difference frequencies at the surge natural frequency, 0.01 Hz, and the pitch natural frequency, 0.032 Hz, have been plotted in FIGURE 9 for comparison. The cylinder has the largest surge-wave-excitation force QTF magnitude, although the magnitudes for all cases are close to 0, for values of the first wave frequencies up to 0.095

Hz, whereas the surge-wave-excitation force QTF magnitude for Configuration 1 dominates at higher wave frequencies.

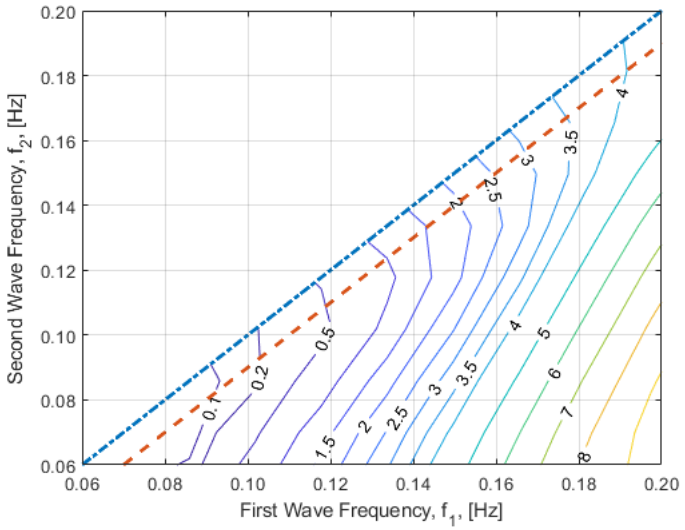

FIGURE 7: SECOND-ORDER SURGE WAVE-EXCITATION FORCE QTF MAGNITUDE FOR ASSEMBLY 1 (AVERAGE PANEL SIZE OF 1 M).

The nondimensional second-order pitch wave-excitation moment QTF magnitude for the cylinder, Assembly 1, and Configuration 1 have been plotted in FIGURE 10, FIGURE 11, and FIGURE 12, respectively. The pitch moment QTF magnitude for the isolated cylinder does not have a maximum peak but rather an increasing gradient when moving from the mean drift force diagonal to the lower-right corner. The addition of the heave plate, in Assembly 1, maintains the same increasing gradient as the cylinder except the maximum value has more than doubled. More interesting results are observed for Configuration 1, wherein a local minima is found in the range between 0.149 and 0.165 Hz for the first wave frequency which maybe the result of an interaction effects from the inclusion of the back columns. This indicates that the wave interaction between the three columns leads to destructive interference that produces a local minimum which is also present in the first-order pitch wave-exciting moment (see FIGURE 5). When comparing the pitch-wave-excitation moment QTF magnitude for bichromatic wave pairs along the pitch natural frequency line, the curves do not overlap like the surge-wave-excitation force QTF magnitude, with the largest increase occurring when comparing Assembly 1 to Configuration 1 (over a five-fold increase in the second-order moment).

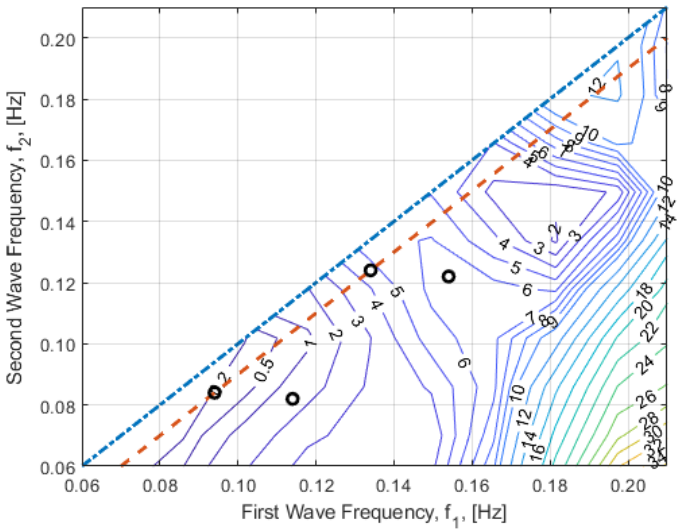

FIGURE 8: SECOND-ORDER SURGE WAVE-EXCITATION FORCE QTF MAGNITUDE FOR CONFIGURATION 1 (AVERAGE PANEL SIZE OF 2 M). THE BLACK CIRCLES INDICATE THE BICHROMATIC WAVE PAIRS CHOSEN FOR THE SIMULATION DEFINED IN SECTION 4.

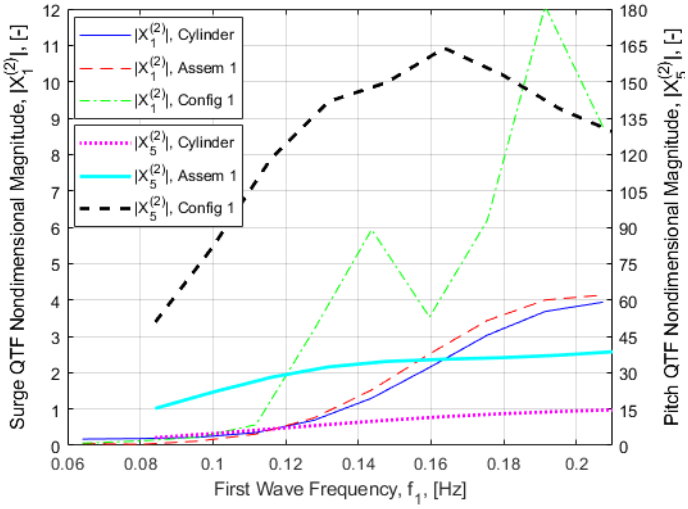

FIGURE 9: COMPARISON OF SECOND-ORDER SURGE-WAVE-EXCITATION FORCE AND PITCH-WAVE-EXCIATION MOMENT QTF MAGNITUDE FOR THE CYLINDER, ASSEMBLY 1, AND CONFIGURATION 1. THE SURGE WAVE-EXCITATION FORCE IS PLOTTED FOR THE BICHROMATIC WAVE PAIRS THAT GENERATE A DIFFRENCE FREQUENCY EQUAL TO THE SURGE NATURAL FREQUENCY. THE PITCH WAVE-EXCITATION MOMENT IS PLOTTED FOR THE BICHROMATIC WAVE PAIRS THAT GENERATE A DIFFRENCE FREQUENCY EQUAL TO THE PITCH NATURAL FREQUENCY.

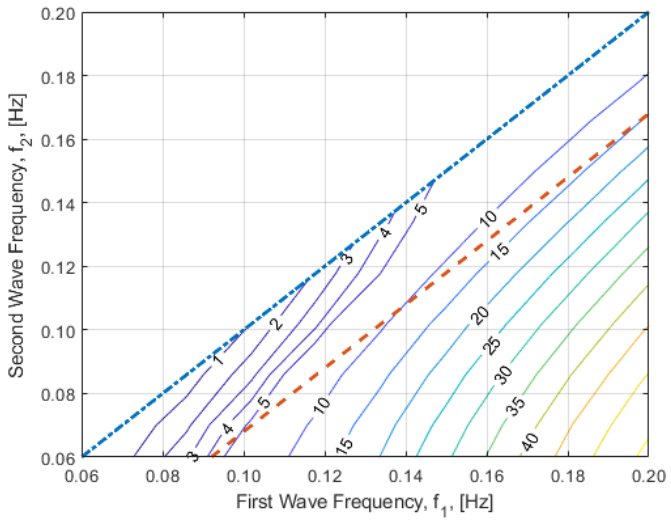

FIGURE 10: SECOND-ORDER PITCH WAVE-EXCITATION-MOMENT QTF MAGNITUDE FOR THE CYLINDER (AVERAGE PANEL SIZE OF 1 M).

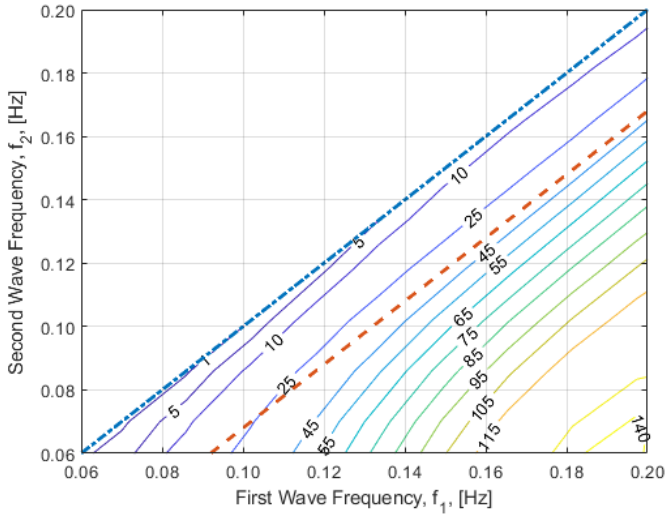

FIGURE 11: SECOND-ORDER PITCH WAVE-EXCITATION MOMENT QTF MAGNITUDE FOR ASSEMBLY 1 (AVERAGE PANEL SIZE OF 1 M).

3.2.2 Convergence of Panel Size on Configuration 1

A convergence study on the panel size was completed to ensure precision in the calculated hydrodynamic diffraction coefficients. Configuration 1 was chosen to for this study and the average panel size was varied until the differences in the reported second-order hydrodynamic diffraction coefficients was minimal. Results for the second-order surge wave-exciting force QTF calculated using a 4-m average panel size has been plotted in FIGURE 13 and can be compared to the calculations using a 2-m average panel size shown in FIGURE 8, with the differences in magnitude plotted in FIGURE 14. As shown in FIGURE 14, the largest difference in the surge wave-exciting force QTF is 0.25, which corresponds to about 10% of the 2-m panel size value at the 0.118 and 0.070 Hz bichromatic wave pair. However, the focus of this paper is to understand the difference frequency QTF forcing along the surge and pitch natural frequencies, which has been plotted in FIGURE 15. This plot shows that along bichromatic wave pairs that produce a difference frequency at the surge natural frequency there is little difference between the 2-m and 4-m panel sizes, and the surge results have converged. However, a larger difference is observed for the second-order-pitch wave-exciting moment QTF with the 2-m average panel size producing larger hydrodynamic forcing. An additional 1-m average panel size WAMIT case is currently being run, but was not ready for paper submission The results of this test case will provide evidence of whether or not the second-order-pitch wave-excitation moment has converged or an even smaller average panel size is required.

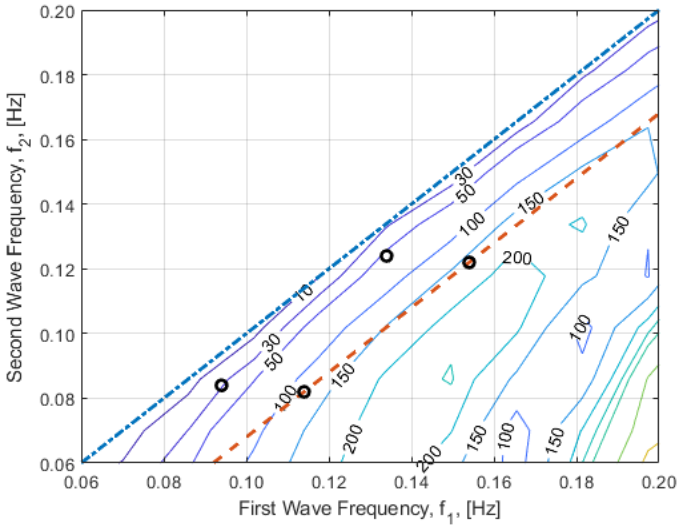

FIGURE 12: SECOND-ORDER PITCH WAVE-EXCITATION MOMENT QTF MAGNITUDE FOR CONFIGURATION 1 (AVERAGE PANEL SIZE OF 2 M) THE BLACK CIRCLES INDICATE THE BICHROMATIC WAVE PAIRS CHOSEN FOR THE SIMULATION DEFINED IN SECTION 4.

3.2.3 Effect of Discretizing the Free Surface

Ignoring the free-surface forcing can be an efficient approximation of the complete second-order solution. We chose this option for obtaining the results shown in Section 3.2.1 and 3.2.2, as these sections were focused on identifying the differences between structural components and panel size. In this section, the effect of discretizing the free surface on the QTFs is explored. WAMIT provides various options to discretize the free surface, but the results presented in this section include the automatic free surface discretization option, which only requires defining the radius of the partition circle, which was set at 50 m.

The free-surface data file of WAMIT contains the information required to perform the integration of the quadratic forcing over the entire free surface exterior to the structures [7]. Near the structure, the integration is carried out by numerical quadratures over the free surface. Away from the structure, the integration can be performed efficiently using asymptotic approximations of the forcing. WAMIT divides the free surface

into two regions by a 'partition circle.' The radius of this partition circle needs to be sufficiently large so that the asymptotic expansion of the forcing is valid outside of the internal surface.

WAMIT does allow users to compute the second-order solution without evaluating the free-surface integral as this is an additional computational effort.

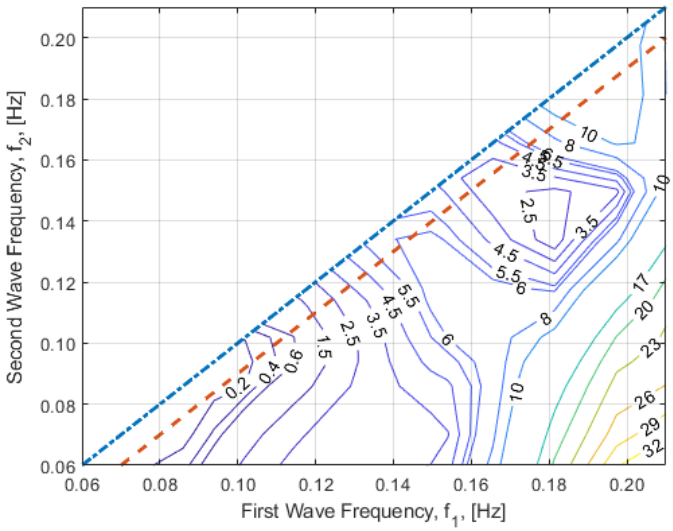

FIGURE 13: SECOND-ORDER-SURGE WAVE-EXCITING-FORCE MAGNITUDE (AVERAGE PANEL SIZE OF 4 M).

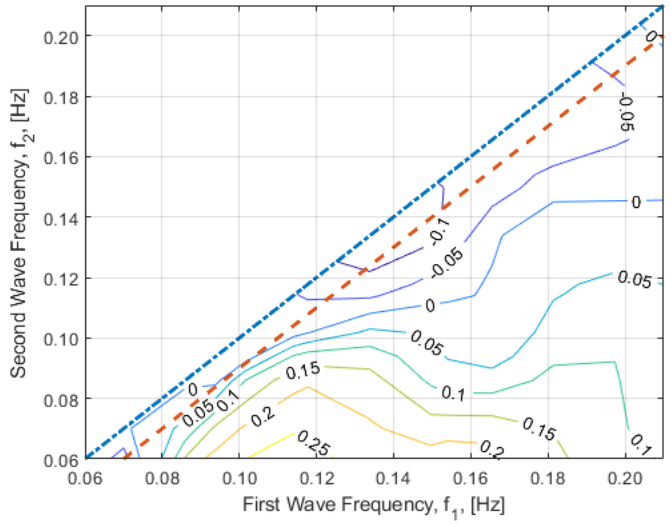

FIGURE 14: DIFFERENCE IN THE SECOND-ORDER-SURGE WAVE-EXCITING- FORCE MAGNITUDE BETWEEN THE 2- AND 4-METERS AVERAGE PANEL SIZES.

For the isolated cylinder, the ratio of the cylinder radius to the partition circle radius is 0.12 and the surge-wave-excitation-force-QTF magnitude is plotted in FIGURE 16, with discretization of the free surface, and can be compared against FIGURE 6, without discretization of the free surface, where the difference in the surge-wave-excitation-QTF force magnitude has been plotted in FIGURE 17. The largest differences in the surge-wave-excitation-force QTF magnitude occur when the first-wave frequency is at the highest value, with the second-wave frequency at the lowest value. The variation is minimal along the red dashed line, which denotes the bichromatic wave pairs that generate a difference frequency equal to the semisubmersible surge natural frequency. The surge-wave-excitation-force QTF magnitude and phase along the surge and pitch natural frequency lines have been plotted in FIGURE 18 and FIGURE 19. The surge-wave-excitation-force and pitch-wave-excitation-moment-QTF magnitude and phase along the difference-frequency lines will be the main contributors to the excitation of the semisubmersible motion at the surge and pitch natural frequencies in an irregular sea state.

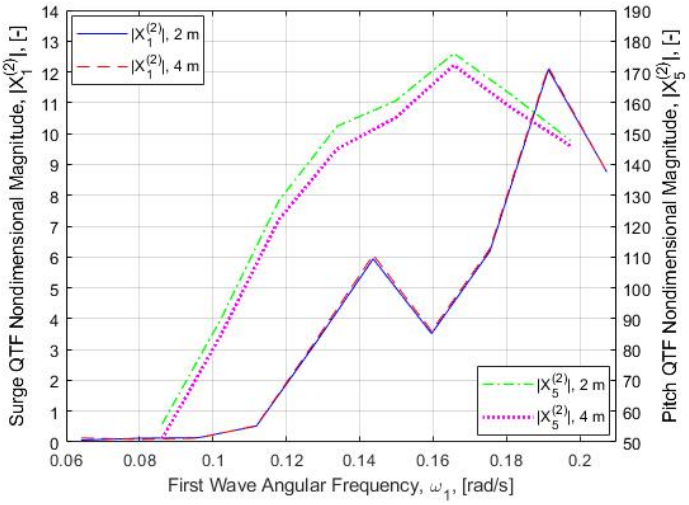

FIGURE 15: COMPARISON OF SECOND-ORDER-SURGE-WAVE-EXCITATION FORCE AND PITCH-WAVE-EXCITATION-MOMENT-QTF MAGNITUDE FOR CONFIGURATION 1 AGAINST THE PANEL SIZE.

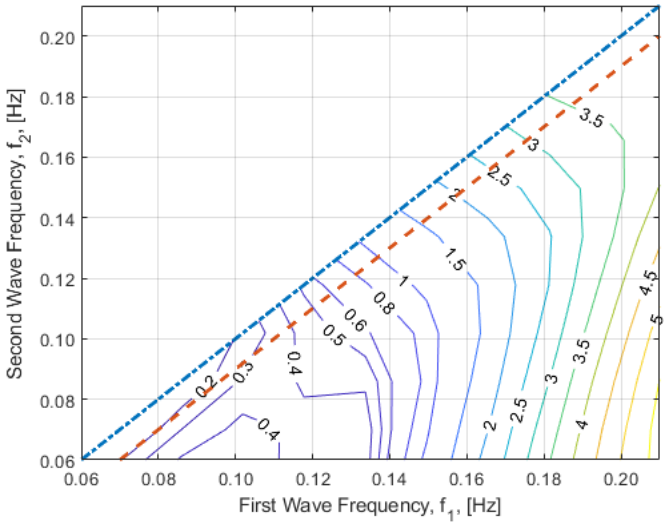

FIGURE 16: SECOND-ORDER-SURGE WAVE-EXCITING-FORCE MAGNITUDE FOR THE CYLINDER WITH A FREE-SURFACE INNER RADIUS OF 50 M AND AVERAGE PANEL SIZE OF 1 M.

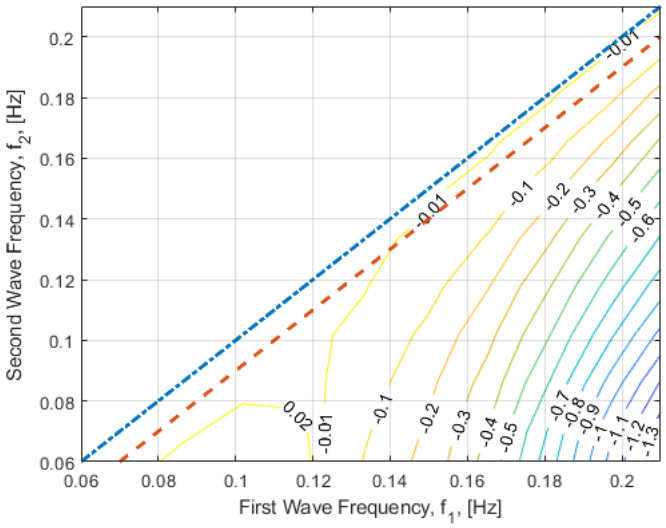

FIGURE 17: DIFFERENCE IN THE SECOND-ORDER-SURGE WAVE-EXCITATION-FORCE MAGNITUDE FOR THE CYLINDER WITH AND WITHOUT DISCRETIZING THE FREE SURFACE (AVERAGE PANEL SIZE OF 1 M).

The WAMIT results show a very minimal difference in the QTFs when discretizing the free surface. The largest difference appears in the pitch-wave-excitation-QTF moment phase, which has the largest visual separation between 0.181 and 0.197 Hz. However, WAMIT does suggest that the radius of the partition circle be on the same order of magnitude as the longest wavelength for deep water to achieve sufficient accuracy. This would require increasing the partition circle radius to 533 m. This will be explored in future work; however, given the results from the cylindrical geometry and the Configuration 1 QTF results, a significant difference may not be observed.

For Configuration 1, the ratio of the characteristic radius to the partition circle radius is 0.69, which shortens the distance between the field points and the fair-field asymptotic expansion. Despite increased concern over validity of the far-field approximation, the surge-wave-excitation-QTF magnitude and phase values along the surge and pitch natural frequency lines show slightly more variation than the cylinder and have been plotted in FIGURE 20 and FIGURE 21. With a more complex geometry, the pitch-QTF moment shows the largest differences in magnitude, which reduce the reported values at the higher wave frequencies. As stated for the single cylinder conditions, additional WAMIT runs will be completed with a larger partition circle radius to improve our understanding of the influence of the free surface.

4 LOAD CASE DEFINITION

The bichromatic wave cases for the new validation campaign were based on the QTF plots for Configuration 1, as shown in FIGURE 8 for surge and FIGURE 12 for pitch. The information in these plots was scaled by an irregular wave spectrum (with a wave height of 7.1 m and peak-spectral frequency at 12.1 s), to identify locations in the QTF that would create the largest forcing during an irregular wave event. Wave- frequency pairs were chosen at locations in the scaled QTF plots, where the values are largest along the difference-frequency lines at the surge and pitch natural frequencies of 0.01 and 0.032 Hz.

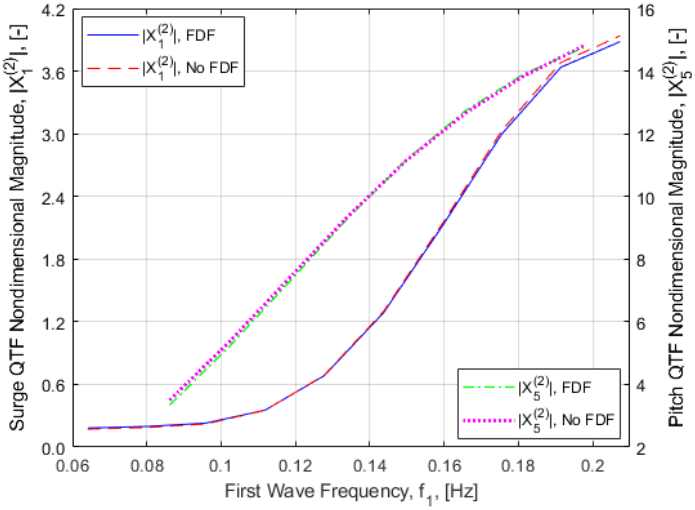

FIGURE 18: COMPARISON OF THE SECOND-ORDER-SURGE WAVE-EXCITATION FORCE AND PITCH-MOMENT MAGNITUDE FOR THE CYLINDER WITH AND WITHOUT A FREE SURFACE OF 50 M AND AVERAGE PANEL SIZE OF 1 M. THE SURGE FORCE IS PLOTTED FOR THE BICHROMATIC WAVE PAIRS THAT GENERATE A DIFFERENCE FREQUENCY EQUAL TO THE SURGE NATURAL FREQUENCY. THE PITCH MOMENT IS PLOTTED FOR THE BICHROMATIC WAVE PAIRS THAT GENERATE A DIFFERENCE FREQUENCY EQUAL TO THE PITCH NATURAL FREQUENCY.

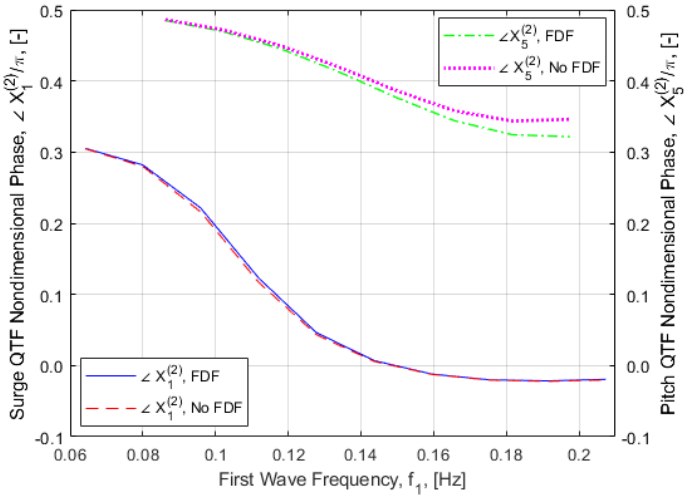

FIGURE 19: COMPARISON OF THE SECOND-ORDER-SURGE-WAVE-EXCITATION FORCE AND PITCH MOMENT PHASE FOR THE CYLINDER WITH AND WITHOUT A FREE SURFACE OF 50 M AND AVERAGE PANEL SIZE OF 1 M. THE SURGE FORCE IS PLOTTED FOR THE BICHROMATIC WAVE PAIRS THAT GENERATE A DIFFERENCE FREQUENCY EQUAL TO THE SURGE NATURAL FREQUENCY. THE PITCH MOMENT IS PLOTTED FOR THE BICHROMATIC WAVE PAIRS THAT GENERATE A DIFFERENCE FREQUENCY EQUAL TO THE PITCH NATURAL FREQUENCY.

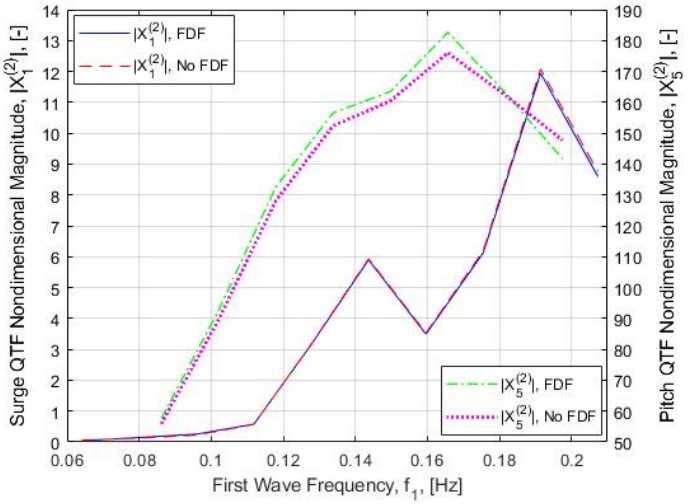

FIGURE 20: COMPARISON OF THE SECOND-ORDER WAVE-EXCITATION-SURGE FORCE AND PITCH-MOMENT PHASE FOR CONFIGURATION 1 WITH AND WITHOUT A FREE-SURFACE RADIUS OF 50 M AND AVERAGE PANEL SIZE OF 2 M. THE SURGE FORCE IS PLOTTED FOR THE BICHROMATIC WAVE PAIRS THAT GENERATE A DIFFERENCE FREQUENCY EQUAL TO THE SURGE NATURAL FREQUENCY. THE PITCH MOMENT IS PLOTTED FOR THE BICHROMATIC WAVE PAIRS THAT GENERATE A DIFFERENCE FREQUENCY EQUAL TO THE PITCH NATURAL FREQUENCY.

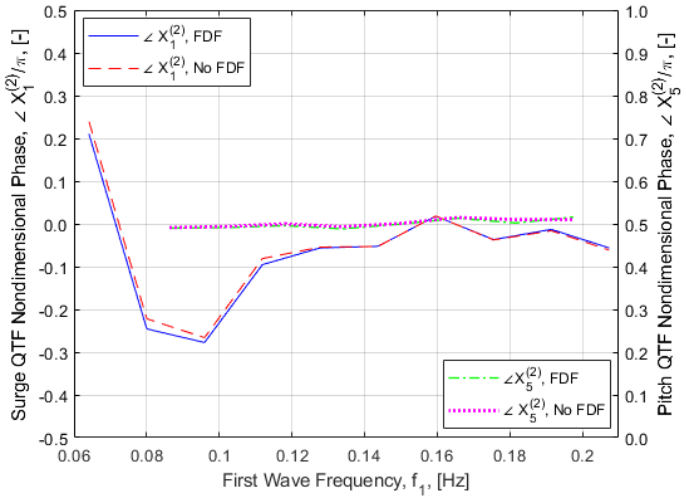

FIGURE 21: COMPARISON OF THE SECOND-ORDER WAVE-EXCITATION-SURGE FORCE AND PITCH-MOMENT PHASE FOR CONFIGURATION 1 WITH AND WITHOUT A FREE SURFACE OF 50 M AND AVERAGE PANEL SIZE OF 2 M. THE SURGE FORCE IS PLOTTED FOR THE BICHROMATIC WAVE PAIRS THAT GENERATE A DIFFERENCE FREQUENCY EQUAL TO THE SURGE NATURAL FREQUENCY. THE PITCH MOMENT IS PLOTTED FOR THE BICHROMATIC WAVE PAIRS THAT GENERATE A DIFFERENCE FREQUENCY EQUAL TO THE PITCH NATURAL FREQUENCY.

Two wave pairs for surge were identified, with frequencies of 0.094/ 0.084 Hz, and 0.134/ 0.124 Hz, both whose difference will create a forcing at 0.01 Hz, which is the surge natural frequency of the OC5-DeepCwind semisubmersible. For the pitch DOF, we selected frequencies of 0.114/0.082 Hz and 0.154/0.122 Hz, which create an excitation at 0.032 Hz—the pitch natural frequency. The wave height is set to 3.5 m for all bichromatic wave components, creating a maximum value of 7 m for the wave height when two waves are added linearly and providing a similar wave height to the irregular-wave spectrum. Additionally, one load case with a smaller height of 2.5 m is considered to investigate whether the derived QTF value would change based on wave amplitude. The load cases are summarized in TABLE 3.

TABLE 3: LOAD CASES

Load Case	Frequency 1 [Hz]	Frequency 2 [Hz]	Difference Frequency [Hz]	Wave Height [m]
1 (surge)	0.094	0.084	0.010	3.5
2 (surge)	0.134	0.124	0.010	3.5
3 (pitch)	0.114	0.082	0.032	3.5
4 (pitch)	0.154	0.122	0.032	3.5
5 (pitch)	0.114	0.082	0.032	2.5

5 OPENFAST SIMULATION RESULTS

In this section, we provide some perspective on the sensitivity of the low-frequency loading on the semisubmersible Configuration 1 using the newly defined bichromatic wave cases. As mentioned previously, there are two primary modeling components contributing to the hydrodynamic loading at the pitch and surge natural frequencies, the nonlinear excitation from the QTFs, and the viscous-drag term of Morison's equation. Section 3 examines the needed components on the QTF side, and this section focuses on the impact of the drag. This analysis will help further guide the needs for the validation campaign.

The impact of the drag modeling choices on the hydrodynamic loading were examined through OpenFAST simulations, which were performed for a simulation time of 1000 s for each of the five bichromatic wave load cases. Four different models were compared to examine the impact of the computation of different drag coefficients on the hydrodynamic force in the x-direction (surge) and the hydrodynamic moment in the y-direction (pitch). The difference between a distributed and calibrated Cd-value versus a simple and uniform Cd value, and the impact of a higher Cd in axial direction is evaluated. For the axial drag values, a baseline value of 9.6 is used as defined by the OC4 project [10] [11]. This value is only placed on the lower surface of the heave plate and is therefore double of a standard Cd value of 4.8.

The following models were compared:

- Model 1: Tuned Cd values (0.4 for the upper columns, 1.6 for the base column, 8.2 in axial direction)
- Model 2: No drag force
- Model 3: Cd value of 1.0 in the transversal direction for all components, and a value of 8.2 in the axial direction
- Model 4: Tuned Cd values in the transversal direction, a higher Cd value of 9.6 in the axial direction

FIGURE 22 shows the amplitude spectrum derived from the time series of the hydrodynamic force in the x-direction for load case 1. The first-order forces have a frequency of 0.094 and 0.084 Hz, the second-order difference-frequency force is found at the difference of these two frequencies: 0.01 Hz. The models with drag forces show hydrodynamic effects of a higher order (other frequencies) because of the computation of the viscous-drag term from Morison's equation, where the water velocity is multiplied by its absolute value. Model 4 is not considered for load case 1 and 2, because the change of an axial Cd has no effect on a force in the x-direction. The effect on the moment is shown in FIGURE 23 for load case 3. The first-order frequencies in load case 3 are at 0.114 and 0.820 Hz, and the second-order difference frequency is at 0.032 Hz.

At the surge and pitch natural frequencies, the magnitudes of the loads of the bichromatic waves are higher than the magnitudes of a full irregular spectrum, with a significant wave height of 7.1 m, a peak period of 12.1 s, and a gamma factor of 3.3, because the energy is concentrated.

FIGURE 24 compares the values of the second-order force at 0.01-Hz difference frequency for load cases 1 and 2. For the force in the x-direction, the impact of the drag forces is significant. The simple drag model with a generic Cd value of 1.0 leads to higher forces, because the total drag force is higher than the force with Cd values calibrated from free-decay tests. For load case 1, a drag coefficient of 1.0 increases the second-order force by more than double (model 3), whereas no drag force decreases the second-order force to only one-third (model 2). For load case 2, the effect is not so extreme; the force with a Cd value of 1 is 23% higher and the force without drag is 13% smaller.

FIGURE 25 shows a comparison of the second-order moments in the y-direction for the four models and the three load cases, focused on the pitch natural frequency. For both bichromatic wave pairs, the second-order moment decreases if drag is not considered (model 2), but only by 2%–3%. Changing the transversal drag coefficient (model 3) or the axial drag coefficient (model 4) does not change the second-order hydrodynamic moment much.

Results from the amplitude spectrum of model 3 can be directly compared to the WAMIT QTF for this specific wave pair. WAMIT QTF data are nondimensional and need to be multiplied by the water density, gravity, and length scale chosen in WAMIT, and the two incident wave amplitudes to provide dimensional forces and moments.

$$F\,[\,in\,N] = QTF \cdot \rho \cdot g \cdot L \cdot A_1 \cdot A_2$$

where ρ is the water density, g is gravity, L is the length scale, and A_1 and A_2 are the amplitudes of each first-order wave component. The OpenFAST simulation results for model 3 were verified to match the QTF entries for the frequency pairs chosen at the surge and pitch natural frequencies. Thus, the process was verified on how the experimental measurements will be used to validate the QTF entries at the chosen locations.

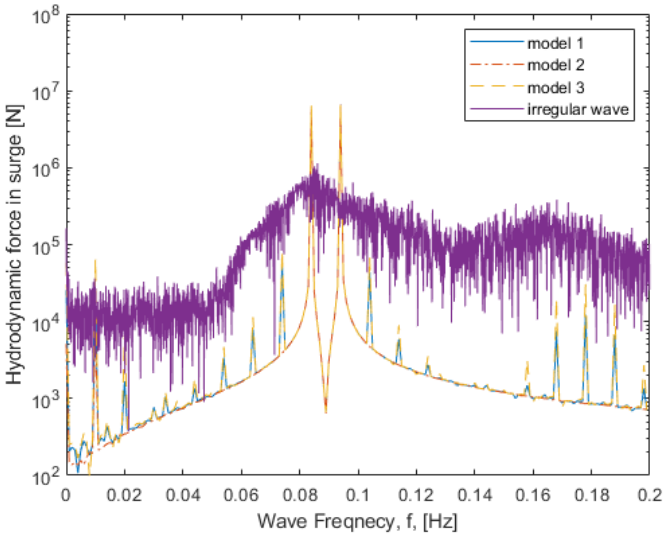

FIGURE 22. AMPLITUDE SPECTRUM OF THE TOTAL HYDRODYNAMIC FORCE IN THE X-DIRECTION FOR LOAD CASE 1 (SEMILOG-Y SCALE)

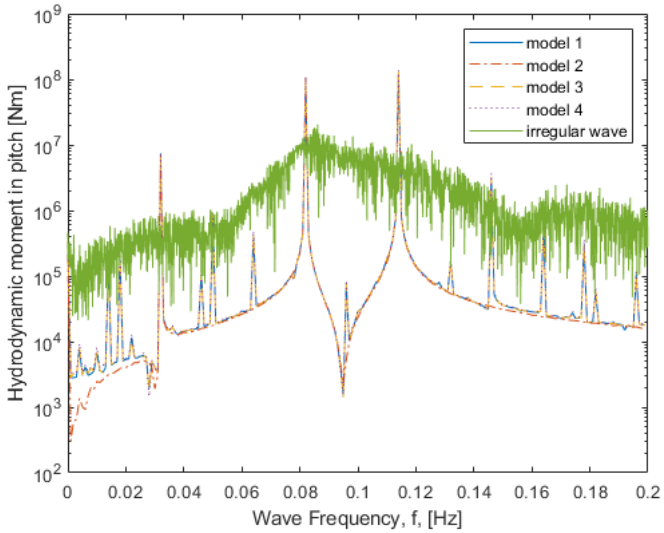

FIGURE 23. AMPLITUDE SPECTRUM OF THE TOTAL HYDRODYNAMIC MOMENT IN THE Y-DIRECTION FOR LOAD CASE 3 (SEMILOG-Y SCALE)

6 CONCLUSIONS

We defined a set of bichromatic wave cases for investigating the second-order hydrodynamic loading on the OC5-DeepCwind semisubmersible. Although irregular wave spectrums are traditionally used for this type of analysis, bichromatic waves have been shown by other researchers to be a good approach for directly validating the components of the QTF, which is one of the primary contributors to this load.

The paper summarizes the procedure used to develop the QTF for components of the OC5-DeepCwind semisubmersible, including the sensitivity of different parameter choices, such as the effect of discretization and modeling the free surface. A set of load cases are then defined by identifying points in the QTF that create the largest contribution to the response at the pitch/surge natural frequencies. The defined wave cases will be

used in a new experimental campaign to be conducted on the components of the OC5-DeepCwind semisubmersible. Because the campaign will examine different combinations of the individual components, the QTF values for the different configurations are also shown.

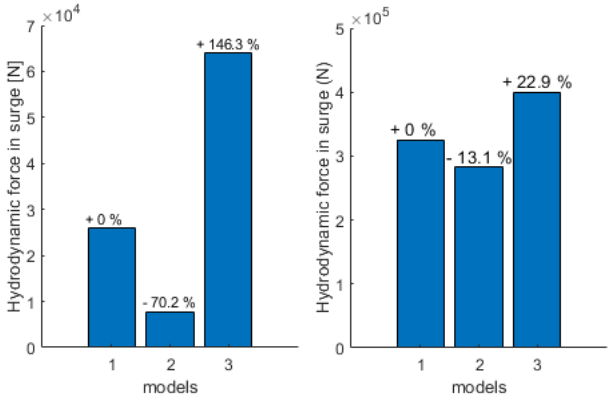

FIGURE 24. SECOND-ORDER FORCE OF LOAD CASE 1 (LEFT) AND LOAD CASE 2 (RIGHT).

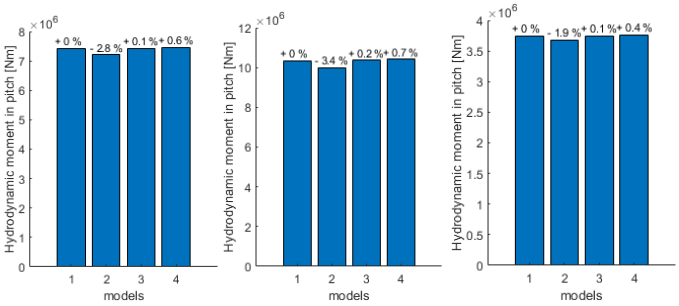

FIGURE 25. SECOND-ORDER MOMENTS OF LOAD CASE 3 (LEFT), LOAD CASE 4 (MIDDLE), AND LOAD CASE 5 (RIGHT).

The proposed approach enables a three-way validation of engineering-level tools such as OpenFAST, along with higher-fidelity CFD tools, where a full irregular wave simulation is impractical computationally. The hydrodynamic loading at the surge and pitch natural frequencies is shown to be sensitive to the drag model in the engineering tools. Examining this drag force using CFD models will be a central focus for understanding the limitations of the engineering models but can only be done if the CFD models can be validated against the wave tank measurements for these bichromatic wave cases. The CFD models can then be used to perform more in-depth investigations beyond what the experimental data can provide, such as examining the loading with and without viscosity considered, and how the nonlinear wave phenomenon behaves at different scales. The validated CFD tool will thus allow for a better understanding of where the engineering models have limited accuracy, with the possibility of finding approaches to either tune or improve these lower-fidelity models.

ACKNOWLEDGEMENTS

This work was authored by the National Renewable Energy Laboratory, operated by Alliance for Sustainable Energy, LLC, for the U. S. Department of Energy (DOE) under Contract No. DE-AC36-08GO28308. Funding provided by the U.S. Department of Energy Office of Energy Efficiency and Renewable Energy Wind Energy Technologies Office. The views expressed in the article do not necessarily represent the views of the DOE or the U.S. Government. The U.S. Government retains and the publisher, by accepting the article for publication, acknowledges that the U.S. Government retains a nonexclusive, paid-up, irrevocable, worldwide license to publish or reproduce the published form of this work, or allow others to do so, for U.S. Government purposes.

REFERENCES

[1] Robertson, A., et al. "OC5 Project Phase II: Validation of Global Loads of the DeepCwind Floating Semisubmersible Wind Turbine." *Energy Procedia*, Vol 137, pp. 38-57, 2017.

[2] Simos, Alexandre N. & Ruggeri, Felipe & Watai, Rafael A. & Souto-Iglesias, Antonio & Lopez-Pavon, Carlos, 2018. "Slow-drift of a floating wind turbine: An assessment of frequency-domain methods based on model tests," *Renewable Energy, vol. 116,* pp 133-154, Sept. 2017.

[3] Shao, Y. and Faltinsen, O. "A numerical study of the second-order wave excitation springing by a higher-order boundary element method." *International Journal of Archit. Ocean Eng*. V 6, pp. 1000-1013, 2014.

[4] You, J. and Faltinsen, O. "A numerical investigation of second-order difference-frequency forces and motions of a moored ship in shallow water." *Journal of Ocean Engineering and Marine Energy,* Vol. 1, Issue 2, pp. 157-179, 2015.

[5] Ohyama, T. and Hsu, J. "Nonlinear wave effect on the slow drift motion of a floating body." *Applied Ocean Research, Vol. 17, Issue 6,* Dec. 1995.

[6] National Renewable Energy Laboratory. NWTC Information Portal (OpenFAST). March 19, 2015. https://nwtc.nrel.gov/OpenFAST (accessed May 10, 2019).

[7] WAMIT, Inc. *WAMIT User Manual Version 6.1, 6.1PC, 6.1S, 6.1S-PC*. Chestnut Hill, MA. 2011.

[8] Sharma, J. and Dean, R. "Second-Order Directional Seas and Associated Wave Forces." *Society of Petroleum Engineers Journal*. January 1979.

[9] Lee, C.-H., Newman, J. N., Kim, M.-H., and Yue, D. K. P. "The computation of second-order wave loads." *Proceedings of the 10 International Conference on Offshore Mechanics and Arctic Engineering*, Stravanger, Norway, June 23-28, 1991.

[10] Robertson, A., Jonkman, J. Masciola, M. and Song, H. "Definition of the Semisubmersible Floating System for Phase II of OC4."*NREL/TP-5000-60601.* Golden, Sept. 2014.

[11] Wendt, F., Robertson, A., Jonkman, J. and Hayman, G. "Verification of New Floating Capabilities in FAST v8" *AIAA SciTech 2015,* Kissimmee, Florida, January 5–9, 2015.